DERIVING INTERNAL WAVE PHASE SPEED IN THE ARCTIC OCEAN FROM SEQUENTIAL SPACEBORNE SAR OBSERVATIONS

I. E. Kozlov [1]*, T. V. Mikhaylichenko [1]

[1] Marine Hydrophysical Institute of RAS, 299011 Sevastopol, Russia - ik@mhi-ras.ru

KEY WORDS: short-period internal waves, phase speed, wave kinematics, Sentinel-1, SAR imaging, Yermak Plateau, Arctic Ocean.

ABSTRACT:

Here we present direct estimates of phase speeds of short-period internal waves (SIWs) in the Arctic Ocean obtained from the analysis of sequential Sentinel-1 A/B SAR images. Analysis of the data near Svalbard in June-September 2018 has shown a peak in SIW observations in August. Three key regions of SIW generation are identified: deep Fram Strait, southern and central parts of Yermak Plateau and shelf regions northwest of Svalbard. Maximal SIW phase speed values are found over the Yermak Plateau and attain 0.84 m/s. Over Fram Strait and on the Svalbard shelf, phase speed values are similar with mean value about 0.2-0.3±0,03 m/s. We note that obtained SIW phase speeds are higher than maximal tidal currents over all three SIWs' observation sites, suggesting their tidal generation and free propagation at subcritical Froude numbers. Comparison of the satellite-based phase speed estimates with theoretical values obtained using a two-layer model and actual hydrology shows a good correspondence for the cases when the time lag between the satellite and the field data is not exceeding one day.

1. INTRODUCTION

Short-period internal waves (SIWs) are an important element of the dynamic structure of the ocean and affect its "average" state through vertical mixing, horizontal and vertical transfer of momentum, energy, tracers and sediments (Zimin et al., 2016; Fer et al., 2020a; Marchenko et al., 2021; Kozlov et al., 2022). They can influence propagation of acoustic signals and underwater operations. An importance of studying SIW field, its spatial characteristics and kinematics in the Arctic Ocean is also related to their effect on sea ice properties and formation of polynyas (Czipott et al., 1991; Morozov and Pisarev, 2004; Kozlov et al., 2017; Carr et al., 2019; Morozov et al., 2019).

Spaceborne SARs are known to be one of the most effective satellite remote sensing devices capable of observing sea surface manifestations of SIWs and so quantify their horizontal 2-D properties, energetics and infer peculiarities of their generation in the coastal ocean regions (da Silva et al., 2007; Lavrova and Mityagina, 2017; Kozlov et al., 2015a).

Phase speed is an important dynamic property of SIW propagation. Traditionally, it is defined my measuring the distance between coherent sequential SIW trains seen in single SAR images assuming that periodicity of the generation of each wave train is equal to the semidiurnal tidal period M_2 dominant over the most of the World Ocean (da Silva et al., 2015). Another approach is based on utilizing close-in-time satellite observations with a short time gap between sequential measurements. The latter was efficiently used for the analysis of SIW kinematics from visible band and passive microwave data in low latitudes (Liu et al., 2014; Hong et al., 2015; Tensubam et al., 2020).

Yet, for the polar ocean regions such estimates were not available up to now. Due to frequent cloudiness and complex illumination conditions, only spaceborne SARs could be effectively used for this task in the Arctic Ocean (Kozlov et al., 2015b, 2022; Morozov et al., 2017). In this work we attempt to close this gap and explore the potential of Sentinel-1 A/B SAR data to retrieve phase speeds of SIWs in the Arctic Ocean. The obtained results are then compared to SIW phase speed estimates made using a two-layer model and actual *in situ* hydrography data.

2. DATA AND METHODS

Here we use sequential Sentinel-1 A/B SAR data covering the area of Fram Strait, the Yermak Plateau and coastal regions of Svalbard from June to September 2018. Due to their polar orbits, Sentinel-1A and Sentinel-1B have high measurement frequency over the high-latitude regions. The latter is ensured by the operation of Sentinel-1 tandem and the mutual geometry of identical polar orbits with a phase shift of 180°. In this case, one satellite is on the day side and the other is on the night side of the orbit. This fact provides the interval between successive Sentinel-1A/B measurements equal to half of the orbital period, T = 98.6 min. As a result, a distinct set of sequential SAR observations with a time lag of about 50 min is available within the latitude band 70–85° N (Kozlov et al., 2020).

Such a short time lag between consecutive measurements and the high spatial resolution of SAR data, O(100 m), provide a unique opportunity to trace the horizontal movement of surface signatures of SIWs and retrieve their linear propagation speed associated with the phase speed of SIWs, C_{sat}.

The general sequence of satellite data processing has the following steps: 1) selection of consecutive Sentinel-1A/B SAR images in the Copernicus Open Access Hub at https://scihub.copernicus.eu; 2) detection of the SIW signatures on the intersecting parts of the paired SAR images in the Sentinels Application Platform (SNAP) program; 3) calculation and mapping of derived SIW phase speeds in Mathworks ©Matlab.

Dual-polarized HH-band data of gridded Level 1 extra-wide-swath (EW) mode medium-resolution (~90 m) products covering an area of about 400 km × 400 km are used for processing and analysis. To estimate the SIW phase speeds from a pair of sequential SAR images, surface signatures of SIWs in the overlapping fragments of both images are identified. Then, curves matching the positions of the leading waves of all SIW trains detected in both images are drawn and their coordinates are saved. The latter allows to estimate the horizontal shifts in the leading waves' positions during a known time interval from

* Corresponding author

which the phase speed of SIWs is determined, as standardly made in the literature (e.g., Liu et al, 2014; Hong et al., 2015).

The analysis of satellite data was carried out as follows. At the first step, for each wave packet observed in both radar images, the position of the leading wave was defined in the form of a curve passing along the region of maximum values of the radar signal due to intense backscattering from breaking wind waves in surface current convergence zones formed under the action of SIWs (Kudryavtsev et al., 2014). Further, on the basis of three perpendicular sections from the initial position of the leading wave on the first radar image to its final position on the second radar image, the average horizontal displacement of the leading wave was determined. The latter was used to calculate the average linear speed of the displacement of the SIW signatures associated with the average phase speed of SIWs.

Assuming that over a short time interval between successive SAR measurements (<1 h) the intensity of the background currents and the SIW speed don't change much, the measurement error of the horizontal shifts of SIW signatures is entirely determined by the spatial resolution of the SAR data. Given the spatial resolution of the SAR images is 88 m × 87 m in the range and azimuth directions, and the time lag between sequential images equals to ~49 min, the phase speed retrieval error (and the lower limit) would be ±90 m/49.3 min, i.e., ±0.03 m/s.

Altogether 40 pairs of sequential Sentinel-1A/B images made from June to September 2018 were analyzed. Figure 1 shows an example of two overlapping SAR images acquired on 1 August 2018. The area of their intersection is about 40% of the total area of a single image allowing to trace the movement of various upper-ocean dynamic processes over the area of nearly 64 000 km^2.

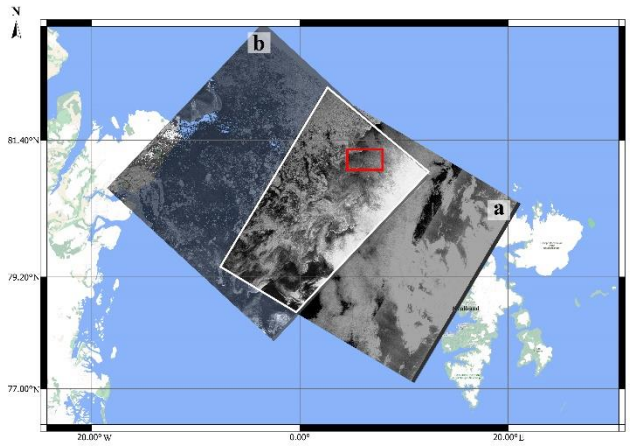

Figure 1. Position of two sequential Sentinel-1A/B images acquired over Fram Strait on 1 August 2018 at a) 07:11 UTC and b) 08:01 UTC. Red rectangle marks the region enlarged in Figure 2.

Figure 2 shows enlarged fragments of both SAR images made on 1 August 2018 exhibiting clear surface signatures of several SIW trains over the southern slope of the Yermak Plateau. The locations, propagation directions and horizontal shifts of leading waves of the four most distinct SIW trains A-D are annotated in Figure 2b. All wave trains travel west-south-west. The mean horizontal shift for the wave train A is about 2 km, for B — 1.6 km, for C — 2 km, for D — 1 km. The mean phase speeds, C_{sat}, for the wave trains A–D are 0.3–0.7 ± 0.03 m/s. The phase speeds of all wave trains considered in the analysis were derived in the same way.

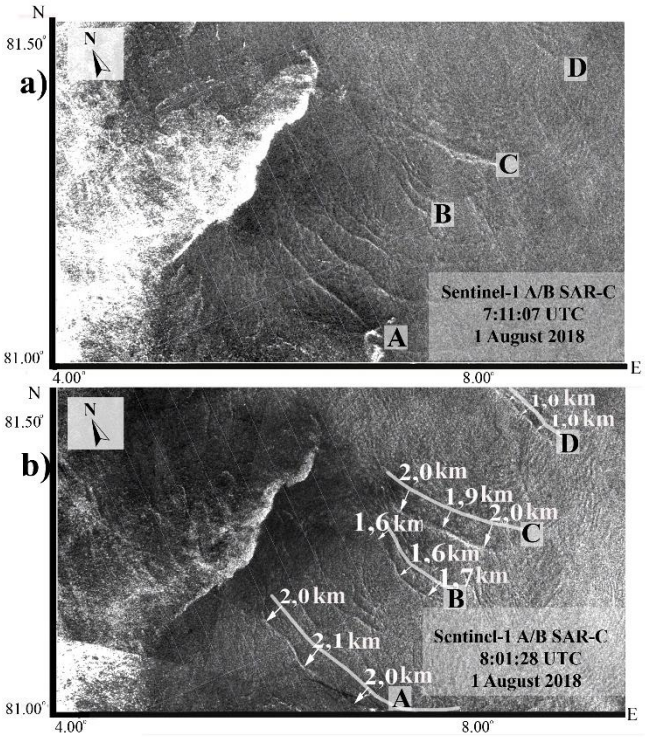

Figure 2. Manifestation of SIW trains in sequential Sentinel-1A/B SAR images acquired on 1 August 2018 over the southern slope of the Yermak Plateau. White lines denote leading waves of four wave trains A-D, arrows show the horizontal shift and direction of SIWs.

3. RESULTS

Analysis of 40 pairs of sequential Sentinel-1 A/B SAR images made from June to September 2018 enabled to detect 231 distinct SIW trains visible in these paired images. It should be noted that a significantly larger number of SIW manifestations (750 SIW signatures) was observed in the initial data. However, due to the difference in the imaging geometry between the Sentinel-1A and the Sentinel-1B satellites (compare a) and b) in Figure 2), SAR signatures of SIWs in one of the paired images could have low radar contrasts for their reliable identification.

The maximum number of SIW signatures (51%) was registered in August, 27% – in July, 12% – in June, and the minimum – in September (10%). Figure 3 presents a generalized map of the spatial distribution of leading waves of all SIW trains detected in the study area in sequential SAR data. Based on Figure 3 it is possible to distinguish three key regions of SIW observations: the deep-sea part of Fram Strait with depths >2000 m (area a), the southern and central parts of the Yermak Plateau with depths of 500–1500 m (area b), and the shelf area northwest of Svalbard with depths <500 m (region c).

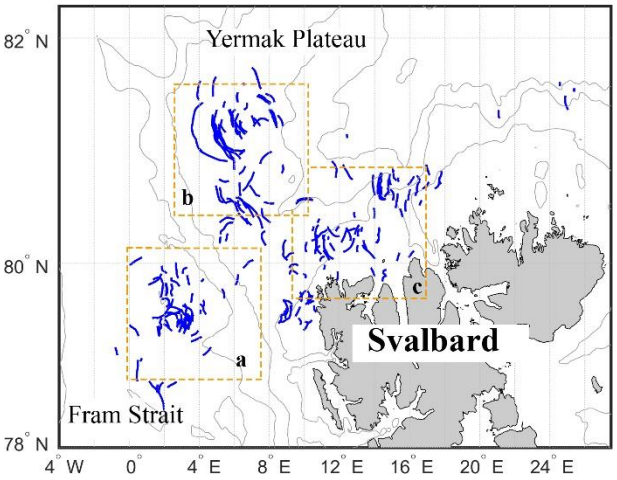

Figure 3. Spatial distribution of leading waves of SIW trains detected in sequential Sentinel-1 A/B images over the study region in June-September 2018.

Figure 4a shows a map of the spatial distribution of the obtained average values of the SIW phase speeds. The range of observed C_{sat} values is 0.08–0.84 ± 0.03 m/s. For the obtained interval of C_{sat} values with an average value of 0.33 m/s, the error in their determination is 4–38% (about 10% for the average value).

As seen, over the deep water of Fram Strait C_{sat} values ranged from 0.2 to 0.4 m/s with an average value of about 0.3 m/s. Significantly higher values of the SIW phase velocity were recorded over the Yermak Plateau. Here they amounted to 0.3–0.8 m/s, including a maximum of 0.84 m/s. On the Svalbard shelf, the range of C_{sat} values was rather high, from 0.1 to 0.8 m/s, but the mean values are also about 0.2-0.3 m/s.

It is interesting to note that the observed difference in the average values of the SIW phase speed between these regions is in general agreement with the spatial inhomogeneity in the tidal current velocity field (see, for example, Figure 1 in (Fer et al., 2020a)). According to Arc5km2018 tidal model (Erofeeva, Egbert, 2020), the maximum velocity of tidal currents in the area of the Yermak Plateau is 0.3–0.6 m/s; near Svalbard - 0.2-0.3 m/s, and over the deep part of Fram Strait - 0.1-0.2 m/s (Fer et al., 2020a).

Regular observations of SIW trains over the same locations suggests they could be generated via the well-known and commonly accepted lee wave mechanism during the interaction of tidal currents with inhomogeneous bottom topography (Vlasenko et al., 2003; Jackson et al., 2012; Fer et al., 2020a). In this case, their kinematic characteristics could be related to the velocity of the tidal currents through the Froude number, $Fr = u/c_0$, where u is the total current velocity; c_0 is the phase velocity of the first-mode IWs. The propagation of internal waves from generation areas is realized at subcritical values of the Froude number, when $Fr < 1$, i.e., when the phase speed of IWs exceeds the velocity of background currents (Jackson et al., 2012). As shown above, the values of the SIW phase speed obtained directly from SAR observations exceed the values of the maximum velocities of tidal currents in all three regions of their observation specified above, which qualitatively confirms the tidal mechanism of their generation and propagation at subcritical values of the Froude number.

The histogram distribution of the average values of SIW phase speed in Figure 4b clearly demonstrates the high probability (about 50% of all observations) of phase speed values in the range of 0.1–0.3 m/s with a pronounced peak for a value of 0.25 m/s. The second peak of observations falls on the phase speed values of about 0.4–0.5 m/s. Values of phase speed exceeding 0.5 m/s occur only in 15% of cases.

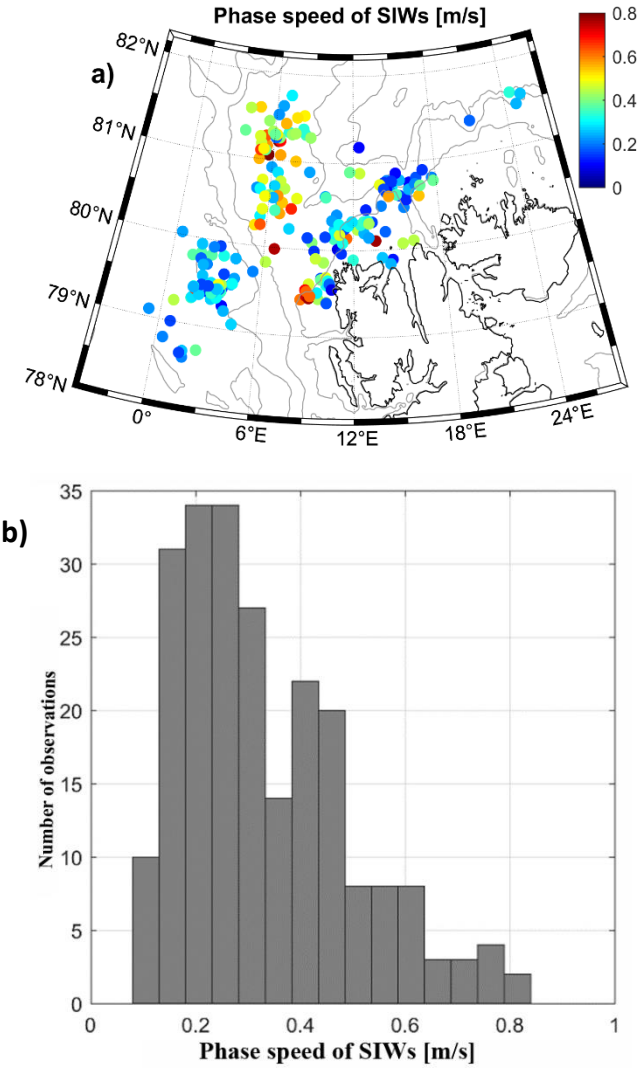

Figure 4. Spatial map (a) and histogram distribution (b) of SIW phase speed values derived from sequential SAR observations in June-September 2018.

The analysis of the distribution histograms for each of the regions a–c shows that they all have several (at least two) main peaks (not shown). The main peak has a minimum value of 0.15 m/s near Svalbard, followed by 0.2 m/s in Fram Strait and 0.3 m/s over the Yermak Plateau. The presence of several peaks in the distribution histograms, apparently, is explained by the seasonal variability of the vertical stratification of waters and the spring-neap cycle of the intensity of tidal currents, leading to the generation of SIWs.

It is important to note that the obtained values of SIW phase speed determined directly from the analysis of satellite data, are, in fact, the sum of the absolute phase speed of the SIWs (C) and the velocity of the background currents (u), including tidal currents. In this regard, it is interesting to compare the observed estimates of the SIW phase velocity (C_{sat}) with the theoretical estimates (C) made on the basis of actual hydrological data. For this task, the results of shipborne CTD measurements made by scientists from the University of Bergen from June 28 to July 10, 2018, near Svalbard are used. The measurement results are described in detail in (Fer et al., 2020b).

Figure 5a shows the location of stations near Svalbard and the locations of SIW manifestations identified in the satellite data during the period of expeditionary work. Figures 5b–5e show

vertical profiles of potential density for several stations taken within sections A, D, T.

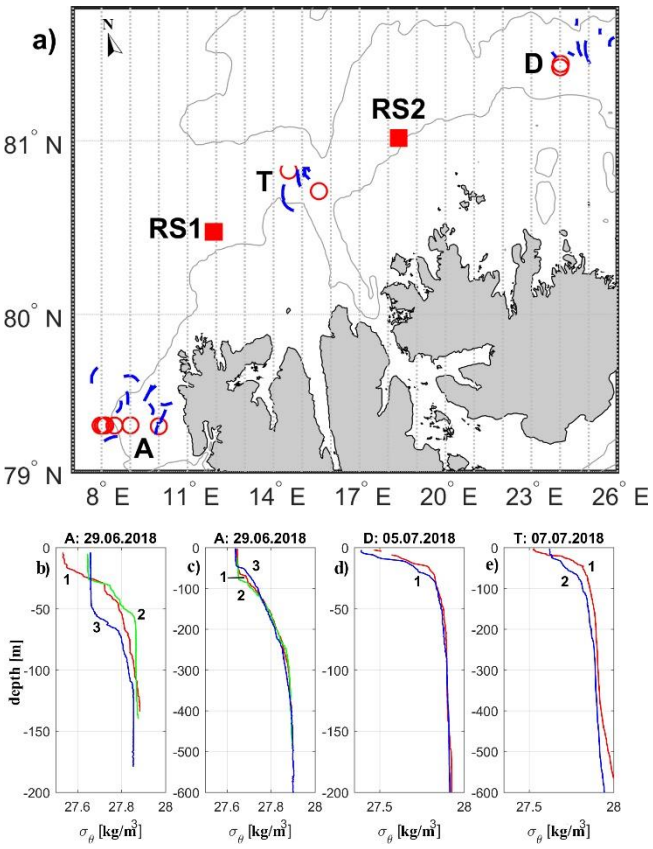

Figure 5. Comparison of satellite SIW observations with *in situ* measurements made near Svalbard in June-July 2018: a) locations of stations along sections A-T (red circles) and leading waves of SIW trains observed nearby (blue lines). b)-d) vertical profiles of potential density at selected stations made along sections A-T.

As can be seen from density profiles shown in Figures 5b–5e, a two-layer model can be satisfactorily used to estimate the phase velocity of the SIWs, as similarly applied e.g., in (Petrusevich et al., 2018; Kozlov et al., 2022). In this case, the phase speed of linear internal waves of the lowest internal mode can be defined as (Phillips, 1977):

$$c_0 = \left(\frac{\delta\rho}{\rho_0}\frac{g}{k}\right)^{1/2}\{\coth kd + \coth k(D-d)\}^{-1/2}, \quad (1)$$

where $\delta\rho$ = density difference between the upper and lower layers

ρ_0 = average density below pycnocline

d = mean pycnocline depth

D = full depth

k = wave number defined as $k = 2\pi/\lambda$, where wavelength λ is taken as a wavelength of the leading waves in ISW trains from SAR observations.

In case of nonlinear internal solitary waves phase speed would be equal to:

$$C = c_0 + \alpha\eta_0/3, \quad (2)$$

where η_0 = amplitude of SIWs

α = coefficient of quadratic nonlinearity defined as:

$$\alpha = {}^3/_2\, c_0(h_1 - h_2)/h_1h_2, \quad (3)$$

where h_1, h_2 = upper- and lower-layer depths, respectively

D = full depth

We will use equations (1)–(3) to calculate the phase speed of the SIWs. According to the field data (Fer et al., 2020a), the amplitude of SIWs recorded at daily stations RS1 and RS2 (see Figure 5a) ranged from 5 to 50 m. The rest of the parameters will be determined from the vertical density profiles. The results of calculations of the absolute values of the SIW phase speed C and their comparison with the data of satellite measurements C_{sat} are presented in Table 1, where for each station the range of C values is determined by the range of SIW amplitudes η_0 = 5–50 m, and the range of C_{sat} values is obtained in the case of observation of several wave trains in the vicinity of a given station or reflects the spatial variability of the phase speed along the front of the leading wave.

St. #	Date in situ	Date SAR	D [m]	d [m]	C [m/s]	C_{sat} [m/s]
A1	29.06	30.06	134	31	**0.26-0.38**	**0,25-0,34**
A1	29.06	05.07	134	31	**0,26-0,38**	**0,36-0,42**
A2	29.06	29.06	149	42	**0,25-0,32**	**0,27-0,33**
A3	29.06	29.06	188	61	**0,24-0,28**	**0,27-0,33**
A3	29.06	05.07	188	61	0,24-0,29	0,34-0,66
A3	29.06	05.07	188	61	0,26-0,30	0,74-0,8
A4	29.06	29.06	397	68	**0,25-0,32**	**0,27-0,33**
A5	29.06	29.06	485	83	**0,25-0,30**	**0,27-0,33**
A6	29.06	05.07	615	49	**0,23-0,32**	**0,3-0,35**
D1	05.07	12.07	281	14	**0,28-0,65**	**0,25-0,39**
T1	07.07	10.07	956	26	0,30-0,53	0,12
T1	07.07	10.07	956	26	0,33-0,58	0,16
T1	07.07	10.07	956	26	0,33-0,59	0,23
A3	07.07	10.07	942	64	0,34-0,42	0,18

Table 1. Comparison of SIW phase speed values obtained north of Svalbard from *in situ* and spaceborne SAR measurements

We note the main features of the results obtained. It can be seen from Table 1 that the best agreement between the observed and absolute values of the SIW phase velocity is obtained for cases where the time difference between satellite and *in situ* measurements is minimal, for example, for surveys made on June 29, 2018 at stations A1–A5 (highlighted in bold in Table 1). In this case, the observed values of the SIW phase speed C_{sat} are, as a rule, somewhat higher than the absolute values of C, but the difference between them does not exceed the error of satellite measurements (±0.03 m/s). On this basis it is difficult to conclude

that there is a systematic addition to the C_{sat} values associated with the background field of surface currents.

It is interesting to note that a good agreement between the SIW phase speed values is also observed for stations A1, A6, D1, despite the fact that satellite measurements were made a week after *in situ* measurements. Yet, the background tidal current velocities at the moment of shipborne and satellite observations were nearly similar, about 6–8 cm/s. The maximum difference in the phase speed values is observed for the T1–T2 stations performed on July 7, 2018. For all the observed SIW trains, the C_{sat} values are two or more times less than predicted by the model. In this case, shipborne measurements were made two days before the neap tide (July 9, 2018), and satellite ones - one day after it. On both of these dates, the amplitude of tidal currents did not exceed 3–4 cm/s, and the waves themselves propagated along the isobaths to the west and southwest. According to the data of ship and satellite measurements, at the time of the satellite imagery, the prevailing wind was about 8–10 m/s of the southwestern direction, i.e., the direction of wind waves and drift currents was actually opposite to the direction of SIW propagation. We, therefore, suggest that this fact can partly explain the noted discrepancy between the model and the satellite estimates of the SIW phase speed.

4. CONCLUSIONS

In this work, we have collected and processed a data set of sequential Sentinel-1A/B images acquired in summer-autumn period of 2018 to directly estimate the phase speed of short-period internal waves in the Arctic Ocean. The analysis of satellite data showed that the main peak of SIW observations in the study region falls on August. Three key regions of the SIW generation are also revealed: the deep-water region of Fram Strait, the southern and central parts of the Yermak Plateau, and the northern shelf of Svalbard.

According to observations, the maximum (average) values of the SIW phase speed are observed over the Yermak Plateau and reach here 0.8 ± 0.03 m/s ($0.5–0.6 \pm 0.03$ m/s). In the other two regions, the phase speed values are close and average at 0.3 ± 0.03 m/s. The observed difference in the average phase speed values between these regions is in good agreement with the spatial inhomogeneity of the tidal currents here.

The observed SIW trains have a regular character and, most likely, are formed during the interaction of tidal currents with inhomogeneous bottom topography. In addition, the observed values of the SIW phase speed usually exceed the values of the maximum velocities of tidal currents in all three regions of their observation, which indirectly confirms their tidal generation via the lee wave mechanism.

Comparison of satellite estimates of the SIW phase speed with theoretical estimates obtained from a two-layer model using quasi-simultaneous hydrological measurements showed the best agreement for cases with a time difference between satellite and *in situ* measurements of no more than one day.

Thus, the analysis of currently available sequential satellite SAR measurements allows not only to determine the sources of internal wave generation and their spatial structure, but also to study their kinematic characteristics and evolution in the Arctic Ocean.

ACKNOWLEDGEMENTS

The study was supported by the Russian Science Foundation grant no. 21-17-00278, https://rscf.ru/project/21-17-00278. The Sentinel-1A/B satellite data was obtained from the archives of the European Maritime Centers system Copernicus Open Access Hub forecasts (https://scihub.copernicus.eu).

REFERENCES

Carr, M., Sutherland P., Haase, A., Evers, K.U., Fer, I., Jensen, A., Kalisch, H., Berntsen, J., Parau, E., Thiem, O., Davies, P.A., 2019. Laboratory experiments on internal solitary waves in ice-covered waters. *Geophysical Research Letters*, 46 (21), 12230-12238. doi.org/10.1029/2019GL084710.

Czipott, P.V., Levine, M.D., Paulson, C.A., Menemenlis, D., Farmer, D.M., Williams, R.G., 1991. Ice flexure forced by internal wave packets in the Arctic Ocean. *Science*, 254 (5033), 832–835.

da Silva, J.C, New, A.L., Azevedo, A., 2007. On the role of SAR for observing "local generation" of internal solitary waves off the Iberian Peninsula. *Canadian Journal of Remote Sensing*, 33(5), 388-403. doi.org/10.5589/m07-041.

da Silva, J.C.B., Buijsman, M.C., Magalhaes, J.M. 2015. Internal waves on the upstream side of a large sill of the Mascarene Ridge: a comprehensive view of their generation mechanisms and evolution. *Deep Sea Research Part I: Oceanographic Research Papers*, 99, 87-104. doi.org/10.1016/j.dsr.2015.01.002.

Erofeeva, S., Egbert, G., 2020: Arc5km2018: Arctic Ocean Inverse Tide Model on a 5-kilometer grid, 2018. doi.org/10.18739/A21R6N14K.

Fer, I., Koenig, Z., Kozlov, I.E., Ostrowski, M., Rippeth, T.P., Padman, L., Bosse, A., Kolas, E., 2020a. Tidally forced lee waves drive turbulent mixing along the Arctic Ocean margins. *Geophysical Research Letters*, 47(16), e2020GL088083. doi.org/10.1029/2020GL088083.

Fer, I., Koenig, Z., Bosse, A., Falck, E., Kolås, E., Nilsen, F., 2020b: Physical oceanography data from the cruise KB2018616 with R.V. Kristine Bonnevie. Dataset. doi.org/10.21335/NMDC-2047975397.

Hong, D.B., Yang, C.S., Ouchi, K., 2015. Estimation of internal wave velocity in the shallow South China Sea using single and multiple satellite images. *Remote Sensing Letters*, 6 (6), 448-457. doi.org/10.1080/2150704X.2015.1034884.

Jackson, C.R.; da Silva, J.C.B.; Jeans, G., 2012. The generation of nonlinear internal waves. *Oceanography*, 25, 108–123.

Kozlov, I., Kudryavtsev, V., Zubkova, E., Atadzhanova, O., Zimin, A., Romanenkov, D., Myasoedov, A., Chapron, B., 2015a. SAR observations of internal waves in the Russian Arctic seas. *IEEE International Geoscience and Remote Sensing Symposium (IGARSS)*, 947-949.

Kozlov, I.E., Kudryavtsev, V.N., Zubkova, E.V., Zimin, A.V., Chapron, B., 2015b. Characteristics of short-period internal waves in the Kara Sea inferred from satellite SAR data. *Izvestiya, Atmospheric and Oceanic Physics*, 51(9), 1073-1087, doi.org/10.1134/S0001433815090121

Kozlov, I.E., Zubkova, E.V., Kudryavtsev, V.N., 2017. Internal solitary waves in the Laptev Sea: first results of spaceborne SAR observations. *IEEE Geoscience and Remote Sensing Letters*, 14(11), 2047-2051. doi.org/10.1109/LGRS.2017.2749681.

Kozlov, I.E., Plotnikov, E.V., Manucharyan, G. E., 2020. Brief Communication: Mesoscale and submesoscale dynamics in the

marginal ice zone from sequential synthetic aperture radar observations. *The Cryosphere*, 14, 2941-2947. doi.org/10.5194/tc-14-2941-2020.

Kozlov, I.E., Atadzhanova, O.A., Zimin, A.V., 2022. Internal solitary waves in the White Sea: hot-spots, structure, and kinematics from multi-sensor observations. *Remote Sensing*, 14, 4948. doi:10.3390/rs14194948

Kudryavtsev, V., Kozlov I., Chapron, B., Johannessen J.A., 2014. Quad-polarization SAR features of ocean currents. *Journal of Geophysical Research: Oceans*, 119 (9), 6046-6065, doi.org/10.1002/2014JC010173.

Lavrova, O., Mityagina, M., 2017. Satellite survey of internal waves in the Black and Caspian Seas. *Remote Sensing*. 9 (9), 892. doi.org/10.3390/rs9090892

Liu, B., Yang, H., Ding, X., Li, X., 2014. Tracking the internal waves in the South China Sea with environmental satellite sun glint images. *Remote Sensing Letters*, 5(7), 609-618, doi.org/10.1080/2150704X.2014.949365.

Marchenko, A.V., Morozov, E.G., Kozlov, I.E., Frey D.I., 2021. High-amplitude internal waves southeast of Spitsbergen. *Continental Shelf Research*, 227, 104523, doi.org/10.1016/j.csr.2021.104523.

Morozov, E.G., Kozlov, I.E., Shchuka, S.A., Frey, D.I., 2017: Internal tide in the Kara Gates Strait. *Oceanology*, 57, 8-18. doi.org/10.1134/S0001437017010106.

Morozov, E. G., Marchenko, A. V., Filchuk, K. V., Kowalik, Z., Marchenko, N.A., Ryzhov, I.V., 2019. Sea ice evolution and internal wave generation due to a tidal jet in a frozen sea. *Applied Ocean Research*, 87, 179-191, doi.org/10.1016/j.apor.2019.03.024.

Morozov, E.G., Pisarev, S.V., 2004. Internal waves and polynya formation in Laptev Sea. *Doklady Earth Sciences*, 398(7), 983-986.

Petrusevich V.Y., Dmitrenko, I.A., Kozlov, I.E., Kirillov, S.A., Kuzyk, Z.Z., Komarov, A.S., Heath, J.P., Barber, D.G., Ehn, J.K., 2018. Tidally-generated internal waves in Southeast Hudson Bay. *Continental Shelf Research*, 167, p.65-76, doi.org/10.1016/j.csr.2018.08.002.

Phillips, O.M., 1977: *The dynamics of the upper ocean*. Cambridge Univ. Press, Cambridge.

Tensubam C.M, Raju, N.J., Dash M.K., Barskar H., 2021. Estimation of internal solitary wave propagation speed in the Andaman Sea using multi–satellite images. *Remote Sensing of Environment*, 252, 112123. doi.org/10.1016/j.rse.2020.112123.

Vlasenko, V., Stashchuk, N., Hutter, K., Sabinin, K. 2003. Nonlinear internal waves forced by tides near the critical latitude. *Deep Sea Research Part I: Oceanographic Research Papers*, 50, 3, 317-338.

Zimin, A.V., Kozlov, I.E., Atadzhanova, O.A., Chapron, B., 2016. Monitoring short-period internal waves in the White Sea. *Izvestiya, Atmospheric and Oceanic Physics*, 52(9), 951–960. doi.org/10.1134/S0001433816090309.